Design and Modeling of the ANFIS-Based MPPT Controller for a Solar Photovoltaic System

Ranganai T. Moyo[1]
Department of Mechanical Engineering,
Durban University of Technology,
Durban 4001, South Africa
e-mail: 21855926@dut4life.ac.za

Pavel Y. Tabakov
Department of Mechanical Engineering and
Institute for Systems Science,
Durban University of Technology,
Durban 4001, South Africa
e-mail: pashat@dut.ac.za

Sibusiso Moyo
Department of Research,
Innovation and Engagement and Institute for
Systems Science,
Durban University of Technology,
Durban 4001, South Africa
e-mail: dvcrie@dut.ac.za

Maximum power point tracking (MPPT) controllers play an important role in improving the efficiency of solar photovoltaic (SPV) modules. These controllers achieve maximum power transfer from PV modules through impedance matching between the PV modules and the load connected. Several MPPT techniques have been proposed for searching the optimal matching between the PV module and load resistance. These techniques vary in complexity, tracking speed, cost, accuracy, sensor, and hardware requirements. This paper presents the design and modeling of the adaptive neuro-fuzzy inference system (ANFIS)-based MPPT controller. The design consists of a PV module, ANFIS reference model, DC–DC boost converter, and the fuzzy logic (FL) power controller for generating the control signal for the converter. The performance of the proposed ANFIS-based MPPT controller is evaluated through simulations in the MATLAB/SIMULINK environment. The simulation results demonstrated the effectiveness of the proposed technique since the controller can extract the maximum available power for both steady-state and varying weather conditions. Moreover, a comparative study between the proposed ANFIS-based MPPT controller and the commonly used, perturbation and observation (P&O) MPPT technique is presented. The simulation results reveal that the proposed ANFIS-based MPPT controller is more efficient than the P&O method since it shows a better dynamic response with few oscillations about the maximum power point (MPP). In addition, the proposed FL power controller for generating the duty cycle of the DC–DC boost converter also gave satisfying results for MPPT.
[DOI: 10.1115/1.4048882]

Keywords: maximum power point tracking (MPPT), adaptive neuro-fuzzy inference system (ANFIS), DC–DC boost converter, solar photovoltaic (SPV) system, perturbation and observation (P&O) method, efficiency, energy, photovoltaics, simulation, solar

1 Introduction

The rapid growth of installed renewable energy sources has shown a significant change in the energy sector with a move to replace traditional power generation sources like coal and diesel with renewable energy sources such as wind and solar [1]. According to the International Renewable Energy Agency (IRENA), the world installed 176 GW of renewable energy capacity in 2020 with solar and wind having a significant contribution [2]. From these statistics, it can be argued that the future is characterized by a mix of energy technologies with renewable energy sources such as solar, wind, and biomass contributing significantly in the new global energy economy. Among the mentioned renewable energy sources, solar photovoltaic (SPV) technology is considered as the most attractive alternative for power generation [3]. The interest in SPV is growing worldwide due to the continuous price drop of both the photovoltaic (PV) modules and solar batteries and the advances in power electronics [4]. However, SPV systems still suffer from relatively low energy conversion efficiency [5]. Currently, the research related to SPV systems is concentrated on solar cell material modification for improving the efficiency, design of efficient maximum power point tracking (MPPT) controllers for extracting maximum available power from PV modules, development of efficient power electronic converters and inverters for stand-alone and grid-connected PV systems, as well as solving power stability and quality issues by developing advanced energy management controllers for hybrid SPV systems. The concept of maximum power point tracking remains an essential technology for improving the efficiency of PV modules. From several studies, it is evident that the use of solar modules without MPPT controllers results in energy wastages, which ultimately results in the need to install more PV modules for the same power requirement [6].

All MPPT techniques have one objective, that is, to force the PV modules always operate at their maximum power point (MPP) for any given weather conditions based on the maximum power transfer theorem (MPTT). The power output of PV modules is characterized by non-linear behavior due to the variation of the solar irradiance and solar cell temperature. For any given weather condition, the solar module's operating point corresponds to a unique point on a current–voltage (I–V) curve. The same unique operating point on the I–V curve also corresponds to a point on the power–voltage (P–V) curve. And the operating point of the PV module must always correspond to the highest value on the P–V curve for the system to generate the maximum power, as shown in Fig. 1. However, if the PV module is connected directly to the electrical load, its operating point is dictated by the load connected, that is, it can take any value on the P–V curve which might not be the MPP, depending on the impedance interaction between PV modules and the connected load. Therefore, MPPT techniques are employed to continuously adjust the impedance seen by the PV module to keep the PV module operating at, or close to, its peak power point under varying solar irradiance, temperature, and load.

Generally, the MPPT controller is composed of a DC–DC power converter which is controlled by an algorithm to drive the panel's operating point to the MPP. The MPPT techniques can be grouped into two categories: conventional techniques, such as perturbation and observation (P&O) [7–9], incremental conductance (InCon) [10,11], and open-circuit voltage (OCV) method [12,13],

[1]Corresponding author.

Contributed by the Solar Energy Division of ASME for publication in the JOURNAL OF SOLAR ENERGY ENGINEERING: INCLUDING WIND ENERGY AND BUILDING ENERGY CONSERVATION. Manuscript received July 13, 2020; final manuscript received October 9, 2020; published online November 18, 2020. Assoc. Editor: Kevin R. Anderson.

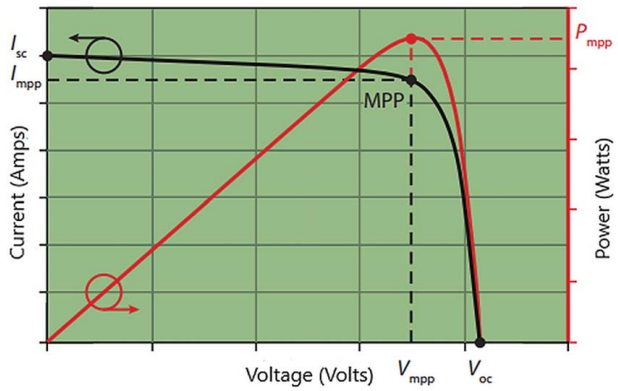

Fig. 1 Current–voltage and power–voltage curves for a PV module [7]

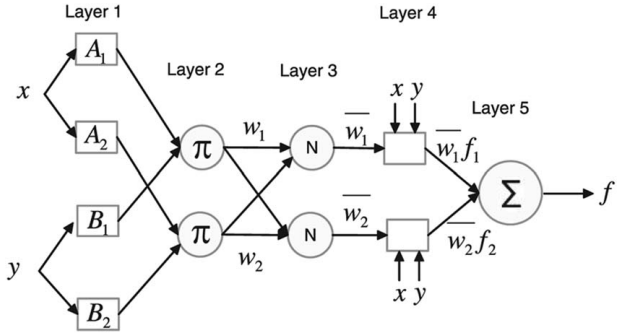

Fig. 2 Adaptive neuro-fuzzy inference system architecture [37]

and based on artificial intelligence (AI) techniques such as artificial neural networks (ANN) [14], fuzzy logic (FL) [15], particle swarm optimization (PSO) [16], and adaptive neuro-fuzzy inference system (ANFIS) [17]. The P&O and InCon are the widely used conventional MPPT techniques because of their simple hardware implementation and sensor requirements as well as low cost. However, as reported in Refs. [18–20], these conventional techniques suffer from various problems such as slow tracking speed, high fluctuations about the MPP, and drift issues involved when there is a rapidly changing weather condition. Also, conventional techniques are defined for uniform environmental conditions and they may fail to track the global maximum power point (GMPP) during nonlinear and partially shaded conditions [21]. Recently, AI-based MPPT techniques have been proposed to address problems associated with conventional MPPT techniques. Amongst them, the FL-based MPPT controller is considered as a powerful one due to its fast-tracking speed and fewer oscillations as reported in Refs. [22–25]. The only challenge with this technique is that it heavily depends on good knowledge about PV systems. Thus, the efficiency of the FL-based controller well depends on the appropriate design of fuzzy rules and memberships functions. The ANN-based MPPT controller is also considered as a powerful technique because of its ability to solve complex and non-linear functions. However, ANN-based MPPT controllers have some drawbacks such as the need for a large amount of training data to ensure accuracy, longer training times, and the complexity in the design of ANN architectures [26]. To solve these limitations, FL can be integrated with ANNs to form an ANFIS for MPPT. The studies [27–30] have proved that ANFIS-based MPPT controllers have a fast dynamic response and small oscillations about the MPP as compared with other MPPT techniques. However, it should be noted that most of the ANFIS-based MPPT controllers that have been presented in the literature rely on the PI(D) controller for generating the duty cycle signal for the DC–DC converter as given in Refs. [17,31–35]. In this study, the FL power controller is proposed for calculation of the duty cycle and for providing a control signal to the DC–DC boost converter. Thus, the proposed ANFIS-based MPPT is made up of a DC–DC boost converter, ANFIS reference model, and FL controller. The ANFIS reference model is trained with a large amount of the real data sets to ensure the accuracy and reliability of the controller.

2 The Architecture of the Adaptive Neuro-Fuzzy Inference System

The ANFIS is a data learning technique that uses FL to transform system inputs into the desired outputs with the use of highly interconnected artificial neural networks, which are weighted to map the numerical inputs into desired outputs [36]. The ANFIS combines the benefits of the two machine learning techniques (backpropagation and least square error algorithms) into a single technique. To demonstrate the ANFIS architecture, two fuzzy IF-THEN rules based on a first-order Sugeno model are considered as follows [37]:

RULE 1: *If* x *is* A_1 *and* y *is* B_1, *then* $f_1 = p_1x + q_1y + r_1$
RULE 2: *If* x *is* A_2 *and* y *is* B_2, *then* $f_2 = p_2x + q_2y + r_2$

where x and y are inputs; A_i and B_i are fuzzy variables; f_i represents outputs within fuzzy sets; p_i, q_i, and r_i are design parameters that are determined during the training process of the ANFIS system. The ANFIS architecture is shown in Fig. 2. In this figure, a circle indicates a fixed node, whereas a square indicates an adaptive node. ANFIS has a five-layer architecture, and the nodes in each layer have similar functions. Each layer is explained in detail below.

Layer 1

The outputs of layer 1 are the fuzzy membership grades of the inputs, which are given by the following equations:

$$O_{1,i} = \mu_{Ai}(x), \quad i = 1, 2 \tag{1}$$

$$O_{1,i} = \mu_{Bi-2}(y), \quad i = 3 \tag{2}$$

where x and y are the inputs to the node i, and Ai and Bi are linguistic labels (high or low) associated with this node functions. $\mu_{Ai}(x)$ and $\mu_{Bi-2}(y)$ can adopt any fuzzy membership function. For example, if the bell-shaped membership function is employed, $\mu_{Ai}(x)$ is given as follows:

$$\mu_{Ai} = \frac{1}{1 + \left[\left(\frac{x - c_i}{a_i}\right)^2\right] b_i}, \quad i = 1, 2 \tag{3}$$

where a_i, b_i, and c_i are parameters of the membership function.

Layer 2

In layer 2, the nodes are fixed nodes. The layer involves fuzzy operators, and it uses the AND operator to fuzzify the inputs. They are labeled with π, indicating that they perform as a simple multiplier. The output of this layer can be represented as

$$O_2, i = w_i = \mu_{Ai}(x) * \mu_{Bi}(y), \quad i = 1, 2 \tag{4}$$

These are the so-called firing strength of the rules.

Layer 3

In layer 3, the nodes are also fixed nodes labeled by N, to indicate that they play the normalization role to the firing strengths from the previous layer. The output of this layer can be represented by

$$O_3, i = \overline{w_i} = \frac{w_i}{w_1 + w_2}, \quad i = 1, 2 \tag{5}$$

Outputs of this layer are called normalized firing strengths.

Layer 4

In layer 4, the nodes are adaptive. The output of each node is simply the product of the normalized firing strength and a first-order polynomial (for a first-order Sugeno model). The output of this layer can be written as follows:

$$O_4,\ i = \overline{w_i} f_i = \overline{w_i}(p_i x + q_i y + r_i), \quad i = 1, 2 \tag{6}$$

where $\bar{w}$ is the output of layer 3 and p_i, q_i, and r_i are the consequent parameters.

Layer 5

In layer 5, there is only one single fixed node labeled with $\sum x$. This node performs the summation of all incoming signals. The overall output of the model is given by

$$O_5,\ i = \sum_i \bar{w} f_i = \frac{\sum_i w_i f_i}{\sum_i w_i} \tag{7}$$

3 System Modeling

3.1 Modeling of the Solar Photovoltaic Module. Photovoltaic is a process of converting solar irradiance into electricity using semiconductor materials that exhibit a property known as the photovoltaic effect [38]. The general model of a solar cell can be derived from the physical characteristics of a diode, which is usually called the single diode model. Figure 3 shows the equivalent circuit for a single diode model. From Fig. 3, the current source, I_L, represents the flow of electrons when solar radiation hits the surface of a solar PV cell. And the diode represents the characteristic behavior of the *PN* junction of the solar PV cell. The model has two resistances, namely, series resistance and parallel resistance. The series resistance (R_s) represents current losses due to metal contacts within the solar PV cells, and the parallel resistance (R_{SH}) accounts for current leakages through the resistive path in parallel with the intrinsic device [17]. Several solar cells have to be connected to form a solar PV module. The output current of the solar PV module is given as

$$I = I_{ph} - I_o[e^{((q(V+IR_s))/(nKN_sT))} - 1] - I_{sh} \tag{8}$$

where I_{ph} is the photo-current; I_o is the saturation current; q is the electron charge; V is the output voltage of the PV module; n is the ideality factor of the diode; K is the Boltzmann constant; N_s represents the number of solar cells connected in series; T is the solar cell temperature; and I_{sh} is the current through the shunt resistor. The current generated from the incidence of radiation at a given temperature is expressed as

$$I_{ph} = \left[I_{sc} + k_i(T - 298)\frac{G}{1000}\right] \tag{9}$$

where I_{sc} represents the short circuit current; k_i is the temperature coefficient of the I_{sc} at standard test conditions (STCs); and G is the solar irradiance. The reverse saturation current of the diode is given by

$$I_{rs} = \frac{I_{sc}}{e^{((q\ V_{oc})/(n\ N_s K\ T))} - 1} \tag{10}$$

where V_{oc} is the open-circuit voltage. The module's saturation current at any given temperature is given by

$$I_o = I_{rs}\left(\frac{T}{T_n}\right)^3 e^{[(q\ E_{go}((1/T_n) - (1/T)))/n\ K]} \tag{11}$$

where $T_n = 298$ K; E_{go} is the bandgap energy. In this study, the ART solar module—360 Wp, 39.0 V Si-monocrystalline type module is used. The parameters of the module at STC are given in Table 1.

By using the parameters presented in Table 1, the MATLAB/SIMULINK model of the solar module is created. After modeling, the MATLAB/SIMULINK PV module model has to be verified or validated to check if resembles the characteristics of the actual module as given in the manufacturer's datasheet. The model is simulated under STCs without connecting any load. STC is a testing condition for manufacturers to check the performance of solar modules, and it specifies that the module must be tested under a solar cell temperature of 25 °C, the irradiance of 1000 W/m^2, and an air mass of 1.5 (AM1.5) [39]. The peak power point of the simulated MATLAB/SIMULINK model was 360 W_p which is given in the manufacturer's datasheet. The *I–V* and *P–V* curves of the simulated MATLAB model of the PV module at 25 °C and different solar irradiance are given in Figs. 4 and 5.

3.2 Proposed ANFIS-Based MPPT Controller. The proposed ANFIS-based MPPT controller is made up of the ANFIS reference model, FL power controller, and a DC–DC boost converter as shown in Fig. 6. This MPPT controller is based on the fact that by knowing the maximum possible power output of a PV module for a given set of solar irradiance and temperature, the real-time MPP of the solar module can be perfectly tracked.

The ANFIS reference model gives out the expected value of the maximum power output from the PV modules at a specific temperature and irradiance. At the same irradiance and temperature, the actual power output which is coming from the PV module is measured and compared with the reference value from the ANFIS model. The difference between the two power values is calculated to give an error, which is then fed to the FL power controller to generate a control signal. The signal generated by the FL power controller is given to the pulse width modulator (PWM). The PWM generates a signal at a high level of frequency to control the duty cycle of the DC–DC power converter and force PV modules to operate at the MPP.

3.2.1 Design of the DC–DC Boost Converter. Maximum power point tracking algorithms are implemented using highly efficient DC–DC power converters. There are several topologies of DC–DC power converters which can be used for maximum power point tracking and these include the boost converter, buck converter, Cùk converter, and SEPIC converter. Because of its

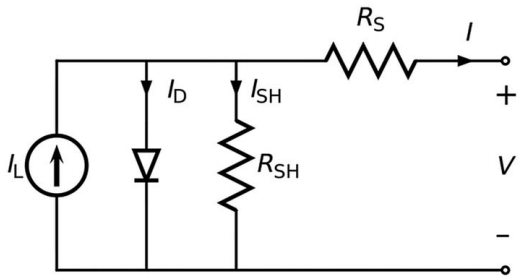

Fig. 3 Equivalent circuit of a single diode model [40]

Table 1 Specifications of the ART-solar-360 Wp

Quantity	Value
Maximum power, P_{MPP}	360 Wp
The voltage at MPP, V_{MPP}	39.0 V
The current at MPP, I_{MPP}	9.24 A
V_{oc}	47.5 V
I_{sc}	9.71 A
Number of cells, N_s	72
Temperature coefficient of the I_{sc}, k_i	0.050%/°C
Temperature coefficient of the P_{max}	−0.39%/°C

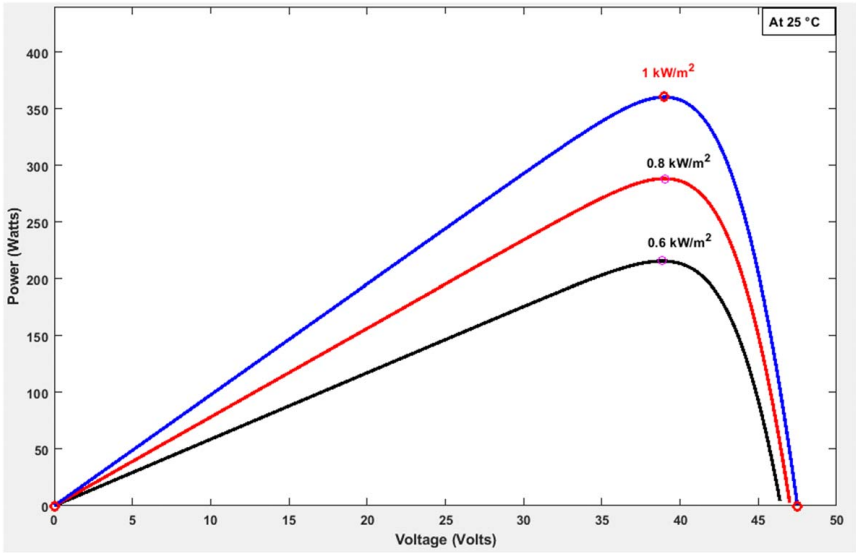

Fig. 4 Power versus voltage curve

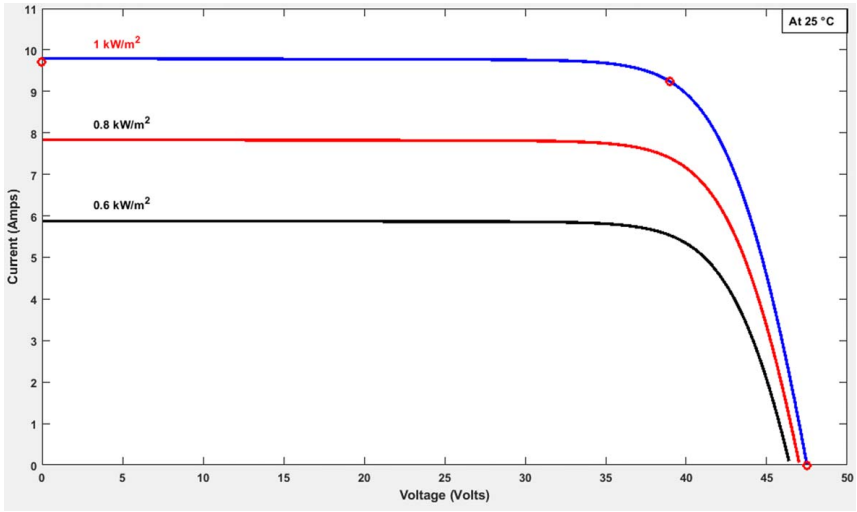

Fig. 5 Current versus voltage curve

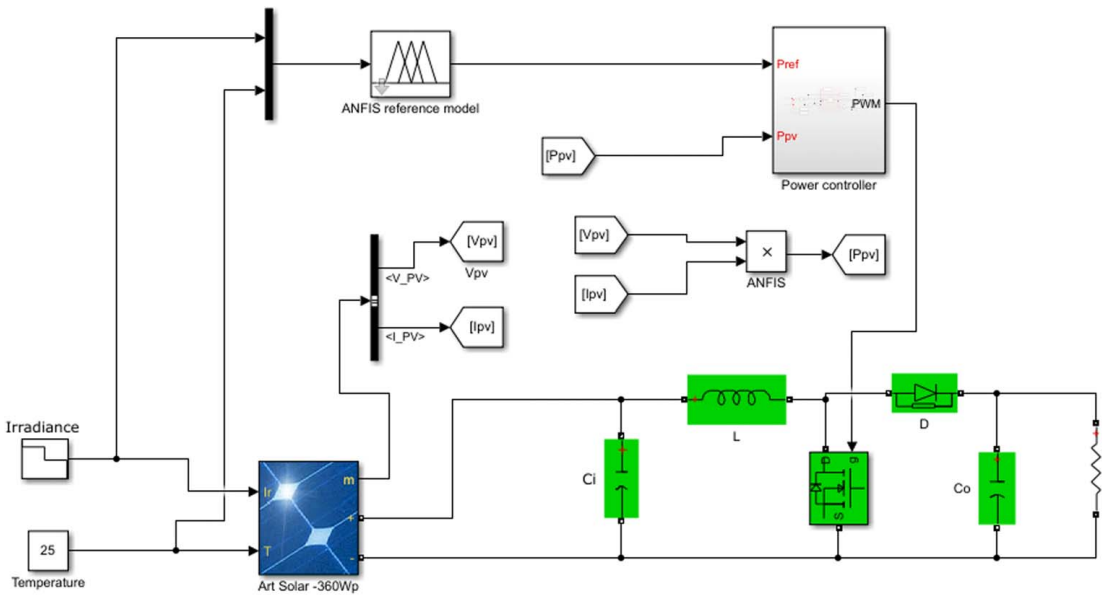

Fig. 6 ANFIS-based MPPT controller

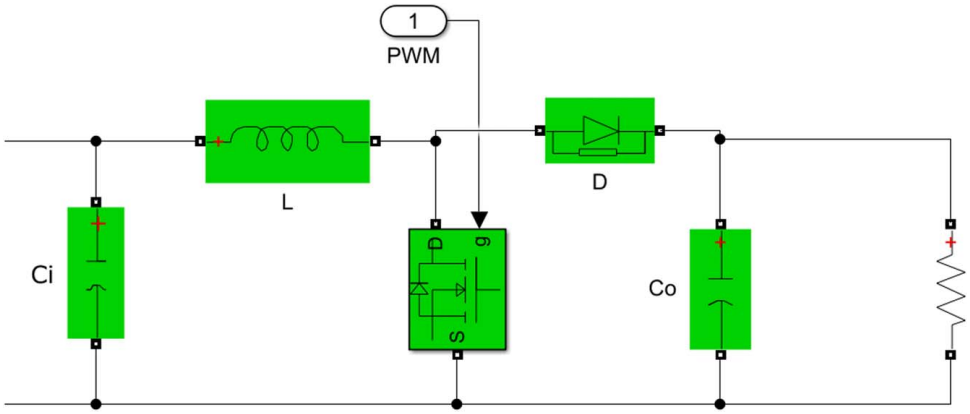

Fig. 7 DC–DC boost converter

Table 2 Selected parameters of the boost converter

Parameter	Symbol	Value
Input voltage	V_{MPP}	39 V
Input current	I_{MPP}	9.24 A
Duty ratio	D_{MPP}	0.35
Inductor	L	3.7 mH
Load resistance	R	10 Ω
Output capacitor	C_o	87.5 μF
Input capacitor	C_i	4000 μF
Switching frequency	f	20 kHz

simplicity and ability to step up the voltage, the boost converted is adopted in this study. A boost converter is made up of two semiconductor switches (diode and MOSFET), an inductor and a capacitor as shown in Fig. 7.

The working principle of the boost converter is based on the fact that the inductor L resists sudden changes in input current. Assuming continuous conduction mode of operation, the converter has two states of operation which are given below.

(a) ON state

During this state, the MOSFET switch S will be on and the diode switch D will be off. The diode will be open-circuited because the n side of the diode will be at higher voltage compared with the p side which will be shorted to the ground. The current flows through the inductor and then to the MOSFET. The inductor stores energy in the form of a magnetic field. On the other side of the circuit, the current flows from the capacitor to the load. The ON state duration is given by $T_{ON} = D + T$, where D is the duty cycle and T is the switching frequency.

(b) OFF state

In this state, the control signal turns off the MOSFET and the diode is turned on. The inductor discharges and the current flows through the diode to the filter capacitor and the load. The capacitor stores energy in the form of charge. The filter capacitor in the output circuit is assumed to be large such that the resistor–capacitor (RC) time constant is higher than the switching frequency to ensure constant output voltage.

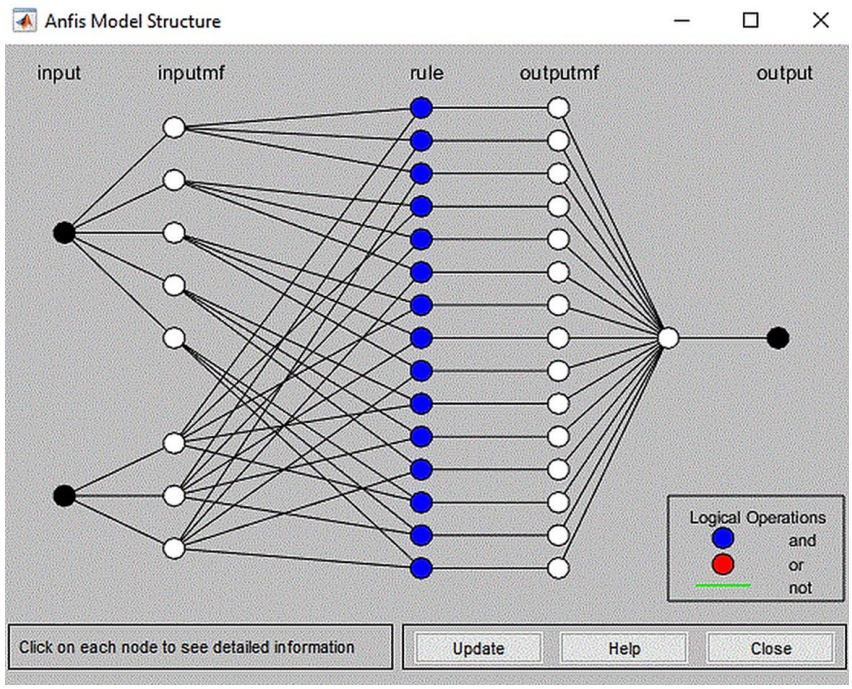

Fig. 8 ANFIS reference model architecture

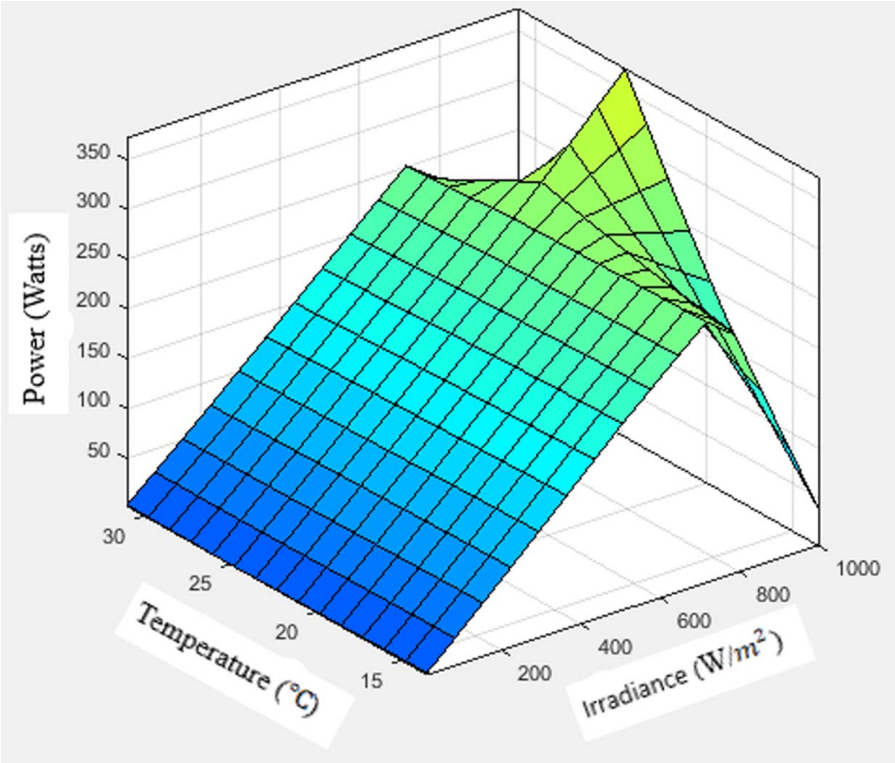

Fig. 9 Surface view of the ANFIS reference model

The boost converter is designed at STC of the solar module. The solar module specifications are given in Table 1. Thus, the PV output current, $I_{PV} = I_{MPP}$, output voltage, $V_{PV} = V_{MPP}$, and output power, $P_{PV} = P_{MPP}$. Therefore, the input/output voltage and current relationships of a DC–DC boost converter are given by

$$V_o = \frac{V_{MPP}}{1 - D} \tag{12}$$

$$I_o = (1 - D) I_{MPP} \tag{13}$$

where V_o is the output voltage of the converter, V_{MPP} is the input voltage to the converter, I_o is the output current of the converter, and I_{MPP} is the input current to the converter. The relationship between the load resistance (R) and optimal internal resistance of the PV module (R_{MPP}) is given as

$$R = \frac{R_{MPP}}{(1 - D_{MPP})^2} \tag{14}$$

where $R = V_o/I_o$, $R_{MPP} = V_{MPP}/I_{MPP}$, and D_{MPP} is the duty cycle

Table 3 Fuzzy rules for the FL power controller

E/*CE*	Very low	Low	Neutral	High	Very high
Very low	VH	VH	H	VL	VL
Low	H	H	H	VL	L
Neutral	H	H	N	L	L
High	H	H	L	L	VL
Very high	H	H	L	L	VL

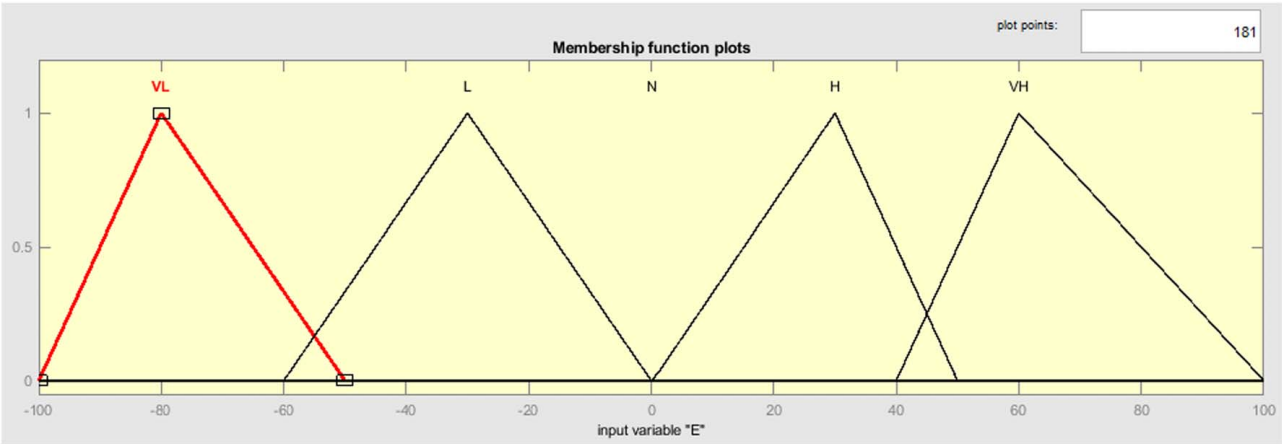

Fig. 10 Membership functions of *E*

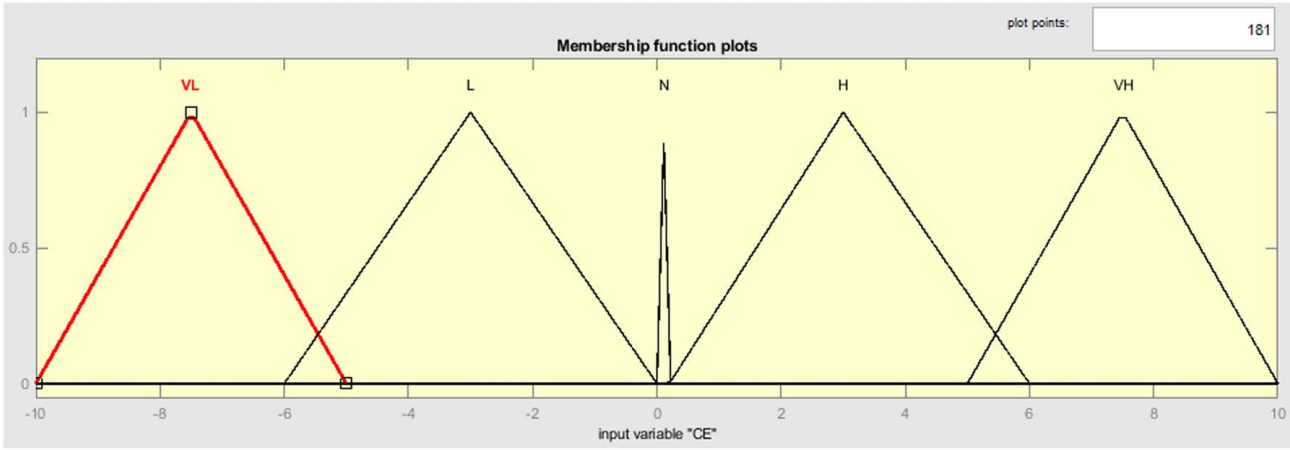

Fig. 11 Membership functions of *CE*

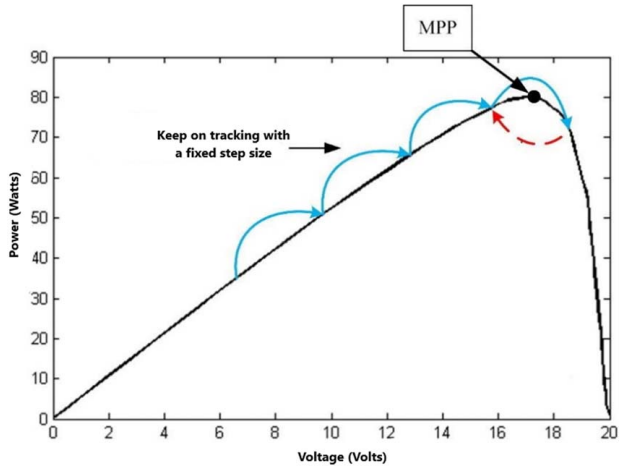

Fig. 12 Illustration of the P&O MPPT technique [20]

at MPP at STC. Since the range of the duty cycle is between 0 and 1, the load resistance must be equal or greater than the optimal internal resistance of the PV module ($R \geq R_{MPP}$). Using the load resistance of 10 Ω and assuming a lossless converter ($P_o = P_{PV}$), the output voltage of the converter is determined as

$$V_o = \sqrt{P_o R} = 60 \text{ V} \tag{15}$$

The duty cycle at MPP at STC is determined as

$$D_{MPP} = 1 - \frac{V_{PV}}{V_0} = 0.35 \tag{16}$$

The PV module's voltage varies with the current and to minimize the ripples, the minimum value of the inductor has to be designed for 1% of current ripples (ΔI_{PV}) at a high-frequency value of 20 kHz as given below [40]

$$L \geq \frac{V_{PV} \times D_{MPP}}{2 \times \Delta I_{PV} \times f} = 3.7 \text{ mH} \tag{17}$$

Additionally, the minimum value of the input capacitor has to be designed for 1% of the voltage ripples as given below [40]

$$C \geq \frac{D_{MPP}}{2 \times \Delta V_o \times f \times R} = 87.5 \ \mu\text{F} \tag{18}$$

In this study, the input capacitor C_i is incorporated to reduce the ripples of the input voltage as well as to deliver alternating current to the inductor. The selected design parameters of the DC–DC boost converter are given in Table 2.

3.2.2 Design of the ANFIS Reference Model. The ANFIS reference model has two input variables (solar irradiance and temperature) and one output variable (reference maximum power output). The temperature and irradiance values for the particular site used in this study have been obtained from the PVGIS website. By simulating the MATLAB/SIMULINK model of the PV module (presented in Table 1) without connecting any load, the reference maximum power output values are generated. The input/output data sets are then used to train the ANFIS reference model. The model was trained with the help of 145 data sets and using triangular membership functions. Figure 8 shows the ANFIS reference model architecture with five membership functions for solar irradiance and three membership functions for temperature.

Figure 9 shows the structure of the surface view plot of the ANFIS reference model, and the mapping between inputs and outputs is demonstrated.

3.2.3 Design of the Power Controller. The power controller is based on FL, and it is used to generate the control signal for the converter. The signal is generated based on the error between the actual power output of the PV module and the reference power output given by the ANFIS reference model. The FL power controller has two input variables (error E and change in error CE) and one output variable (duty cycle increment ΔD). Triangular membership functions were used for each variable in the design of the FL

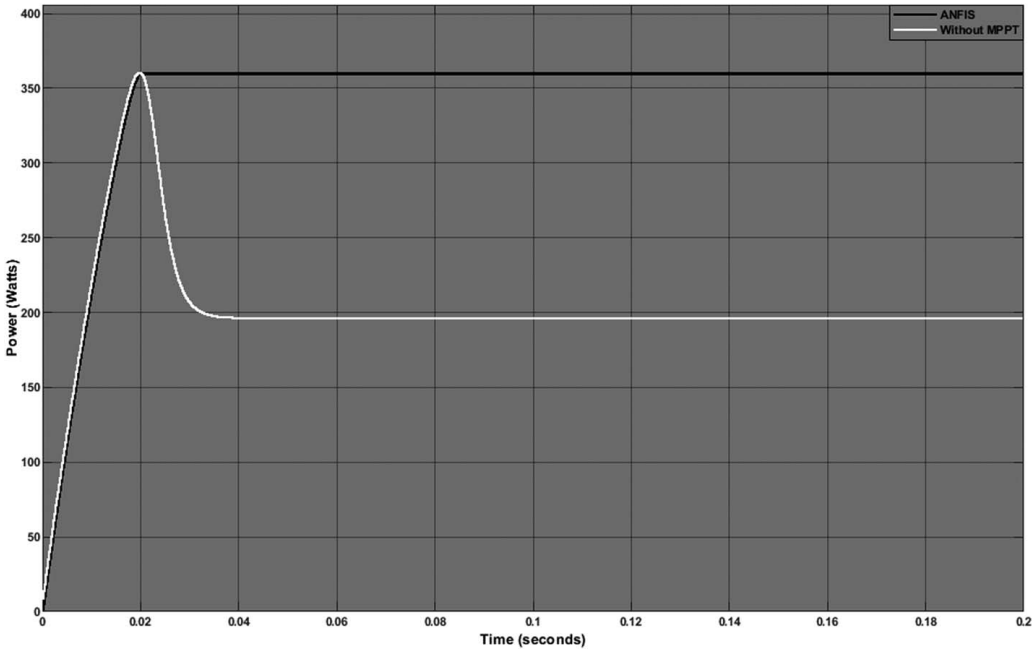

Fig. 13 At STC, with and without the proposed MPPT controller

controller. Five membership functions were chosen for each variable and defined as: Very Low (VL), Low (L), Neutral (N), High (H), and Very High (VH). The ranges of the variables are given as E (−100 to 100), CE (−1 to 1), and D (−0.1 to 0.1).

The controller is designed with 25 fuzzy rules shown in Table 3. Rows and columns represent the input variables (E) and (CE), and the output variable (ΔD) is located at the intersection of the row and the column (Figs. 10 and 11).

3.2.4 Design of the Perturbation and Observation MPPT Controller. The P&O MPPT technique is the widely used MPPT method for improving the efficiency of SPV modules. In this technique, a perturbation is first introduced to the operating voltage of the PV module. The PV module's power output after the perturbation is then calculated and compared with the previous power output. The difference in the two power output values (ΔP) is calculated and if the ΔP is greater than zero, the perturbation is kept in that direction. When ΔP becomes less than zero, the perturbation is reversed and this process is repeated until the MPP is reached. Figure 12 illustrates the P&O MPPT technique.

In this paper, the P&O MPPT technique is for comparison with the proposed ANFIS-based MPPT technique. The P&O MPPT technique is explained in detail in Refs. [9,19,41–44].

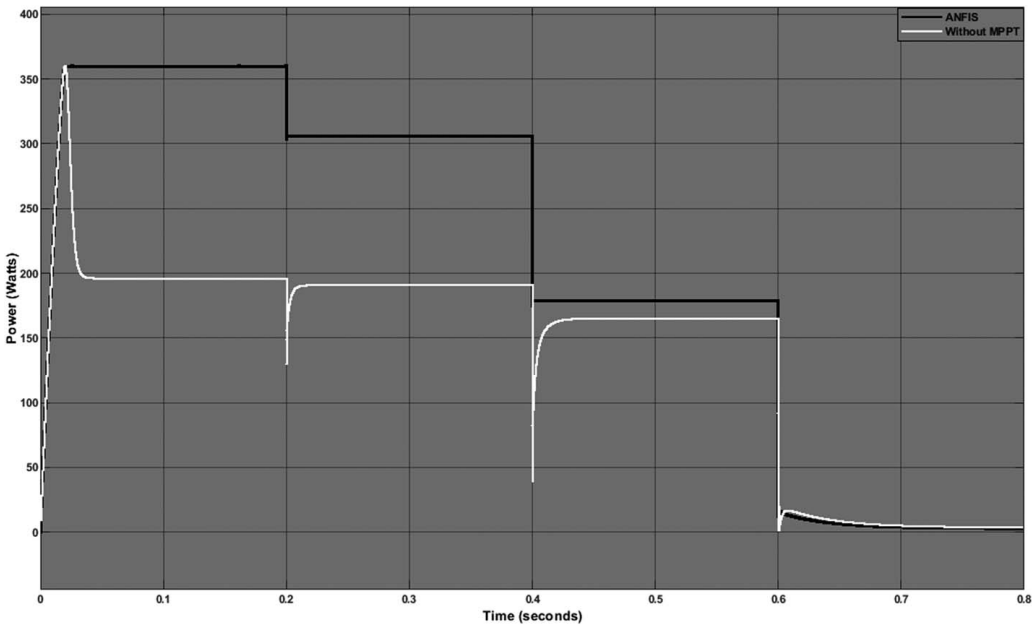

Fig. 14 Under varying solar irradiance, with and without the proposed MPPT controller

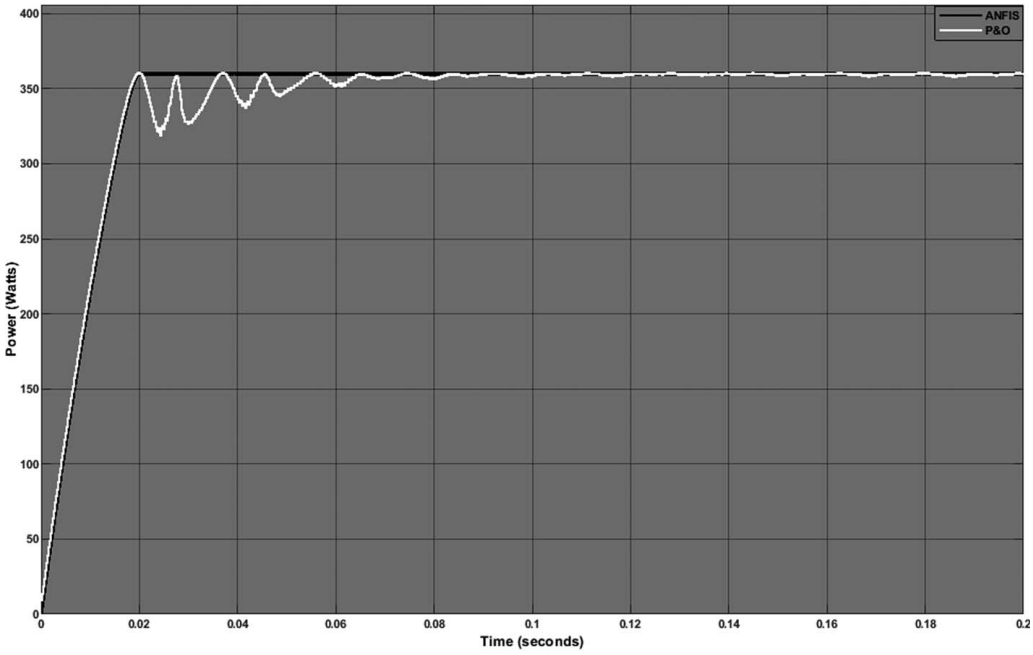

Fig. 15 At STC, comparing with the P&O MPPT controller

4 Simulation Results and Discussion

As stated before, if the PV module is connected directly to the load, its operating point is rarely at the MPP. MPPT techniques are employed to match the internal resistance of the PV module to the load resistance for maximum power to be transferred to the load. To analyze the dynamic behavior of the proposed ANFIS-based MPPT controller, different scenarios were considered and simulated in the MATLAB/SIMULINK environment.

Scenario 1: At STC, with and without the proposed MPPT controller

The proposed MPPT controller is simulated at STC (1000 W/m^2 and 25 °C) and then compared with the simulation of the same circuit but without the MPPT controller. Figure 13 shows the PV module power output with the proposed MPPT (black line) and without the MPPT controller (white line). In both graphs, the PV power output rises sharply from zero up to about the MPP (360 W) after a time of 20 ms. For the system with the MPPT controller, the power output settles at MPP since the MPPT controller will be continuously forcing the PV module to operate at the MPP. For the system without the controller, the PV power

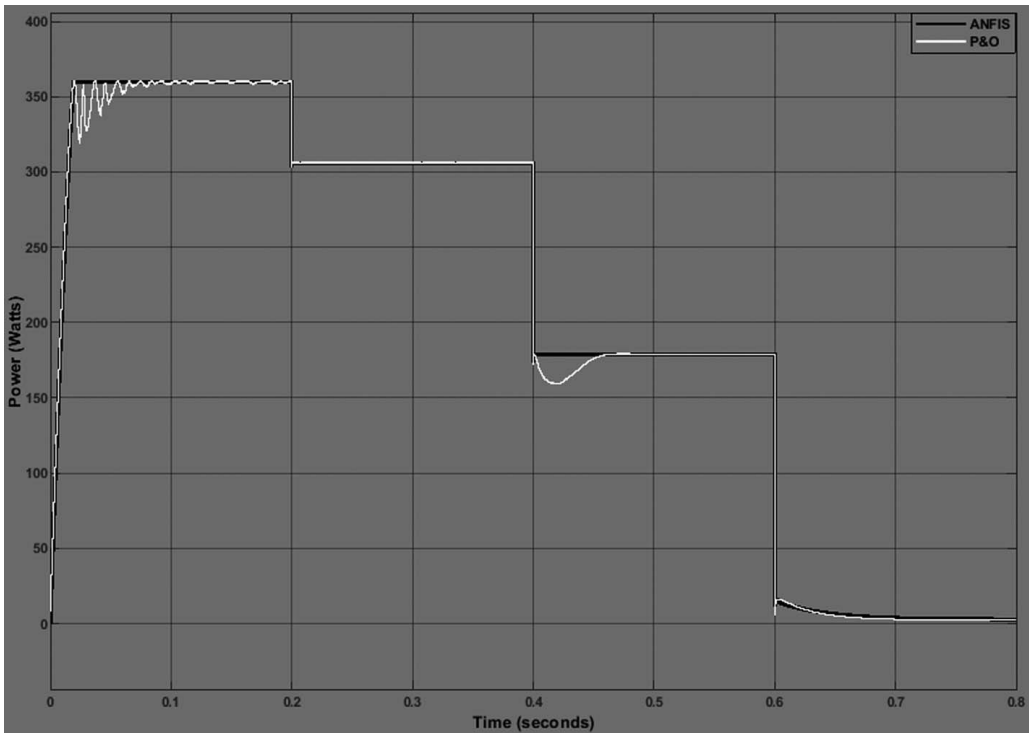

Fig. 16 Under varying solar irradiance, comparing with the P&O MPPT controller

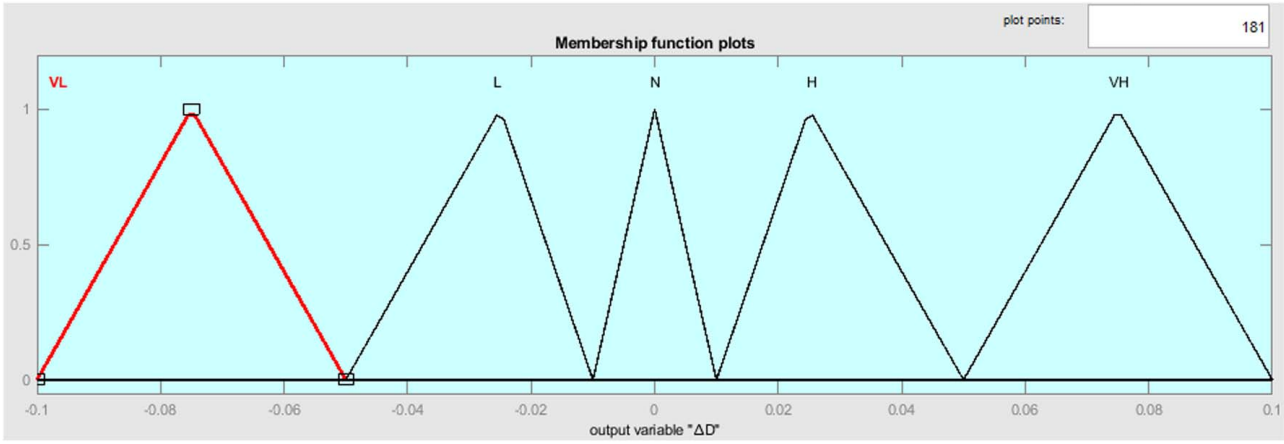

Fig. 17 Membership functions of ΔD

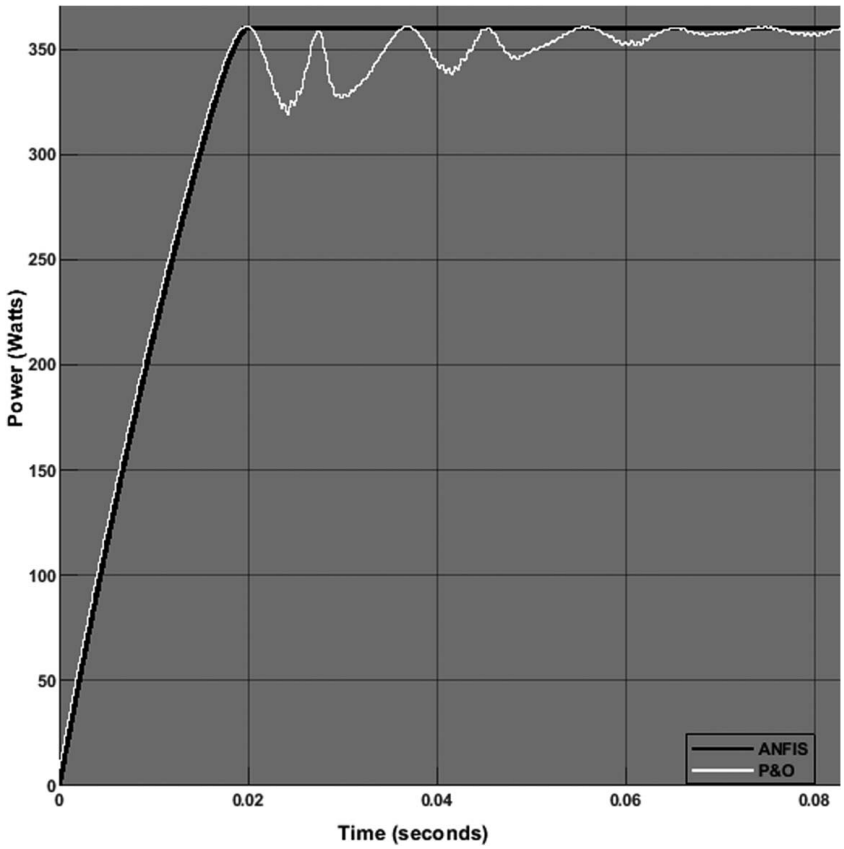

Fig. 18 Zoomed view of the oscillations of the P&O MPPT controller

output drops and settles at around 200 W. This is because the load resistance does not match the internal resistance of the module and there is no external circuit which can force the PV to find its MPP.

Scenario 2: Under varying irradiance, with and without the proposed MPPT

In this case, the proposed controller is evaluated with an operating temperature of 25 °C and sudden changes in solar irradiance (1000 W/m^2, 850 W/m^2, 500 W/m^2, and 50 W/m^2).

Figure 14 shows the PV power output curves for the two systems. It can be noted that the proposed MPPT controller presents a good performance under varying solar irradiance since it perfectly tracks the MPP for different solar irradiances levels. For the PV module without the MPPT controller, the system does not operate at the MPP. However, it should be noted that between 0.4 s and 0.8 s, the system without the controller operates around the MPP. This is because, during that period, the optimal internal resistance of

Table 4 Data sets of solar irradiance and temperature

Solar irradiance (W/m^2)	Temperature (°C)
633	30.6
440	25.2
222	20.1
30	15.2

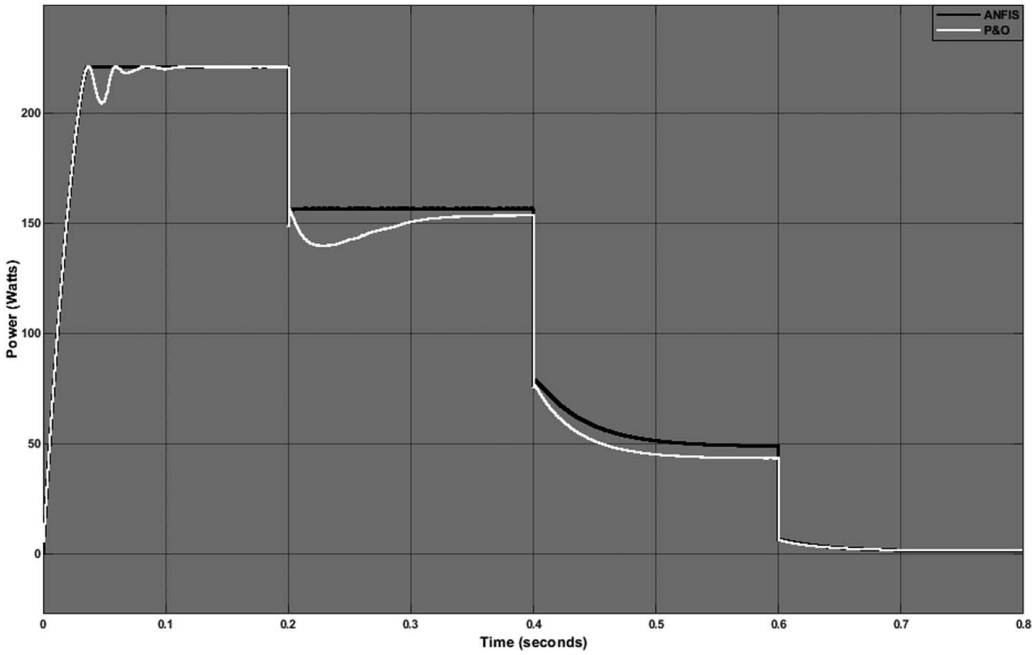

Fig. 19 Under varying solar irradiance, varying temperature comparing with the P&O MPPT controller

the solar module is almost equal to the load resistance of the circuit. At 25 °C, 500 W/m^2, the optimal internal resistance of the PV module is given by

$$R_{\mathrm{MPP}} = \frac{V_{\mathrm{MPP}}^2}{P_{\mathrm{MPP}}} = 8.5\,\Omega$$

Which is almost equal to the load resistance of 10 Ω. Because of that, the PV module can operate at almost MPP without the inclusion of any controller to control its operating point.

Scenario 3: At STC, comparing with the P&O MPPT controller

The performance of the proposed ANFIS-based MPPT controller is also evaluated by comparing it with the P&O MPPT technique at STC. It can be noted from Fig. 15 that for both MPPT controllers, the PV module power output rises sharply up to the MPP with the rise time of 20 ms. For the system with the ANFIS-based MPPT controller, the power output settles and maintains that value. However, for the system with the P&O MPPT controller, the power output oscillates about the MPP before settling down. The power output of the P&O technique settles at the MPP after 80 ms as shown in Fig. 15.

Scenario 4: Under varying solar irradiance, comparing with the P&O MPPT controller

At this point, the performance of the proposed MPPT controller is evaluated by comparing it with the P&O MPPT controller under varying solar irradiance levels (1000 W/m^2, 850 W/m^2, 500 W/m^2, and 50 W/m^2).

Both controllers exhibit satisfactory tracking performance, but the degree of accuracy is different as shown in Fig. 16. The ANFIS-based MPPT controller displays a fast response to sudden changes in solar irradiance levels with small oscillations about the MPPT. For the P&O MPPT controller, the tracking speed is lower and oscillations are much higher. The P&O MPPT controller also exhibits the drift phenomenon (caused by the incorrect decision to either decrease or increase the duty cycle for fast-changing irradiance levels). It must be also noted that the efficiency of the P&O MPPT technique is very poor for lower solar irradiance level (at 500 W/m^2) as illustrated in Fig. 16 (between 40 and 60 ms). This is because the P&O method uses a fixed step to either decrease or increase the duty cycle (non-adaptive) but for the ANFIS-based MPPT controller, ΔD changes (from −0.1 to 0.1 as shown in Fig. 17) depending on the error given to the FL power controller, which makes the proposed MPPT technique efficient for any given solar irradiance level and temperature (Fig. 18).

Scenario 5: Under varying solar irradiance, varying temperature and comparing with the P&O MPPT controller

The performance of the proposed ANFIS-based MPPT is also evaluated under varying solar irradiance and temperature by comparing it with the P&O MPPT technique. In general, the efficiency of PV modules decreases with an increase in solar cell temperature. Four real environmental data sets of solar irradiance and temperature are used. Table 4 shows these data sets.

Figure 19 shows the power output curves of the two controllers. The proposed ANFIS-based MPPT shows a better response for changing solar irradiance and temperature. For the P&O MPPT controller, the accuracy and tracking speed is slower and this results in power wastages since the SPV system will not be operating at the MPP. The reason for this poor performance is because the P&O technique relies on fixed steps to update the duty cycle of the DC–DC boost converter and it takes time for this controller to locate the new MPP for rapidly changing environmental conditions.

5 Conclusion

The design, modeling, and evaluation of the proposed ANFIS-based MPPT controller were presented in this paper. By knowing the maximum possible power output of a PV module for a given set of solar irradiance and temperature, the real-time MPP of the solar module was thoroughly tracked. The components and the subsystems of the proposed MPPT controller were modeled and simulated in MATLAB/SIMULINK environment. The proposed MPPT controller was evaluated by comparing it with a circuit without the MPPT controller as well as with the P&O MPPT technique. Simulation results reveal that the proposed ANFIS-based MPPT can effectively track the maximum power point of PV modules under different weather conditions with the same level of consistency. The proposed FL power controller which was used to generate the control signal to the boost converter also gave satisfying results for MPPT.

Acknowledgment

The authors would like to thank the National Research Foundation of South Africa (NRF) and the Durban University of Technology for their financial support.

Conflict of Interest

There are no conflicts of interest.

References

[1] Owusu, P. A., and Asumadu-Sarkodie, S., 2016, "A Review of Renewable Energy Sources, Sustainability Issues and Climate Change Mitigation," Cogent Eng., **3**(1), pp. 1–14.
[2] I.-I. R. E. Agency. "Renewables Account for Almost Three Quarters of New Capacity in 2019," IRENA, https://www.irena.org/newsroom/pressreleases/2020/Apr/Renewables-Account-for-Almost-Three-Quarters-of-New-Capacity-in-2019, Accessed 2020.
[3] Ahmadi, M. H., Ghazvini, M., Sadeghzadeh, M., Nazari, M. A., Kumar, R., Naeimi, A., and Ming, T., 2018, "Solar Power Technology for Electricity Generation: A Critical Review," Energy Sci. Eng., **6**(5), pp. 340–361.
[4] Malinowski, M., Leon, J., and Abu-Rub, H., 2017, "Solar Photovoltaic and Thermal Energy Systems: Current Technology and Future Trends," Proc. IEEE, **105**(11), pp. 1–15.
[5] Hossain, J., and Mahmud, A., 2014, *Renewable Energy Integration: Challenges and Solutions*, Springer Science & Business Media, New York, p. 1.
[6] Rosu-Hamzescu, M., and Oprea, S., 2013, "Practical Guide to Implementing Solar Panel MPPT Algorithms," Microchip Technology Inc.
[7] Sharma, D., and Purohit, G., 2012, "Advanced Perturbation and Observation (P&O) Based Maximum Power Point Tracking (MPPT) of a Solar Photo-Voltaic System" 2012 IEEE India International Conference on Power Electronics (IICPE), Delhi, India, Dec. 6–8.
[8] Sweidan, T. O., and Widyan, M. S., 2017, "Perturbation and Observation as MPPT Algorithm Applied on the Transient Analysis of PV-Powered DC Series Motor," 8th International Renewable Energy Congress (IREC), Amman, Jordan, Mar. 21–23, pp. 1–6.
[9] Kamran, M., Mudassar, M., Fazal, M. R., Asghar, M. U., Bilal, M., and Asghar, R., 2018, "Implementation of Improved Perturb & Observe MPPT Technique With Confined Search Space for Standalone Photovoltaic System," J. King Saud Univ.—Eng. Sci., **32**(1), pp. 432–441.
[10] Putri, R. I., Wibowo, S., and Rifa'i, M., 2015, "Maximum Power Point Tracking for Photovoltaic Using Incremental Conductance Method," Energy Procedia, **68**, pp. 22–30.
[11] Safari, A., and Mekhilef, S., 2011, "Incremental Conductance MPPT Method for PV Systems," 24th Canadian Conference on Electrical and Computer Engineering(CCECE), Niagara Falls, ON, Canada, May 8–11, pp. 000345–000347.
[12] Das, P., 2016, "Maximum Power Tracking Based Open Circuit Voltage Method for PV System," Energy Procedia, **90**, pp. 2–13.
[13] Ch, S. B., Kumari, J., and Kullayappa, T., 2011, "Design and Analysis of Open Circuit Voltage Based Maximum Power Point Tracking for Photovoltaic System," Int. J. Adv. Sci. Technol., **2**, pp. 51–60.
[14] Dzung, P. Q., Le Dinh, K., Hong Hee, L., Le Minh, P., and Nguyen Truong Dan, V., 2010, "The New MPPT Algorithm Using ANN-Based PV," International Forum on Strategic Technology, Ulsan, South Korea, Oct. 13–15, pp. 402–407.
[15] Mahamudul, H., Saad, M., and Ibrahim Henk, M., 2013, "Photovoltaic System Modeling With Fuzzy Logic Based Maximum Power Point Tracking Algorithm," Int. J. Photoenergy, **2013**, p. 762946.
[16] Liu, Y., Huang, S., Huang, J., and Liang, W., 2012, "A Particle Swarm Optimization-Based Maximum Power Point Tracking Algorithm for PV Systems Operating Under Partially Shaded Conditions," IEEE Trans. Energy Convers., **27**(4), pp. 1027–1035.
[17] Aldair, A. A., Obed, A. A., and Halihal, A. F., 2018, "Design and Implementation of ANFIS-Reference Model Controller Based MPPT Using FPGA for Photovoltaic System," Renew. Sustain. Energy Rev., **82**, pp. 2202–2217.
[18] D'Souza, N. S., Lopes, L. A., and Liu, X., 2010, "Comparative Study of Variable Size Perturbation and Observation Maximum Power Point Trackers for PV Systems," Electric Power Syst. Res., **80**(3), pp. 296–305.
[19] Kamala Devi, V., Premkumar, K., Bisharathu Beevi, A., and Ramaiyer, S., 2017, "A Modified Perturb & Observe MPPT Technique to Tackle Steady State and Rapidly Varying Atmospheric Conditions," Sol. Energy, **157**, pp. 419–426.
[20] Kumar, A., Chaudhary, P., and Rizwan, M., 2015, "Development of Fuzzy Logic Based MPPT Controller for PV System at Varying Meteorological Parameters," 2015 Annual IEEE India Conference (INDICON), New Delhi, India, Dec. 17–20, pp. 1–6.
[21] Lyden, S., and Haque, M. E., 2015, "Maximum Power Point Tracking Techniques for Photovoltaic Systems: A Comprehensive Review and Comparative Analysis," Renew. Sustain. Energy Rev., **52**, pp. 1504–1518.
[22] Ben Salah, C., and Ouali, M., 2011, "Comparison of Fuzzy Logic and Neural Network in Maximum Power Point Tracker for PV Systems," Electric Power Syst. Res., **81**(1), pp. 43–50.
[23] Gupta, A., Kumar, P., Pachauri, R. K., and Chauhan, Y. K., 2014, "Performance Analysis of Neural Network and Fuzzy Logic Based MPPT Techniques for Solar PV Systems," 2014 6th IEEE Power India International Conference (PIICON), Delhi, India, Dec. 5–7, IEEE, pp. 1–6.
[24] Chim, C. S., Neelakantan, P., Yoong, H. P., and Teo, K. T. K., 2011, "Fuzzy Logic Based MPPT for Photovoltaic Modules Influenced by Solar Irradiation and Cell Temperature," 2011 UkSim 13th International Conference on Computer Modelling and Simulation, Cambridge, UK, Mar. 30–Apr. 1, IEEE, pp. 376–381.
[25] Menniti, D., Pinnarelli, A., and Brusco, G., 2011, "Implementation of a Novel Fuzzy-Logic Based MPPT for Grid-Connected Photovoltaic Generation System," 2011 IEEE Trondheim PowerTech, Trondheim, Norway, June 19–23, IEEE, pp. 1–7.
[26] Jiang, L. L., Nayanasiri, D. R., Maskell, D. L., and Vilathgamuwa, D. M., 2015, "A Hybrid Maximum Power Point Tracking for Partially Shaded Photovoltaic Systems in the Tropics," Renew. Energy, **76**, pp. 53–65.
[27] Khaehintung, N., Sirisuk, P., and Kurutach, W., 2003, "A Novel ANFIS Controller for Maximum Power Point Tracking in Photovoltaic Systems," The Fifth International Conference on Power Electronics and Drive Systems (PEDS), Singapore, Nov. 17–20, pp. 833–836, Vol. 2.
[28] Khosrojerdi, F., Taheri, S., and Cretu, A., 2016, "An Adaptive Neuro-Fuzzy Inference System-Based MPPT Controller for Photovoltaic Arrays," 2016 IEEE Electrical Power and Energy Conference (EPEC), Ottawa, ON, Canada, Oct. 12–14, pp. 1–6.
[29] Noman, A. M., Addoweesh, K. E., and Alolah, A. I., 2017, "Simulation and Practical Implementation of ANFIS-Based MPPT Method for PV Applications Using Isolated Ćuk Converter," Int. J. Photoenergy, **2017**, p. 3106734.
[30] Sarhan, M. A., Ding, M., Chen, X., and Wu, M., 2017, "Performance Study of Neural Network and ANFIS Based MPPT Methods For Grid Connected PV System," Proceedings of the 2017 VI International Conference on Network, Communication and Computing, Kunming, China, December.
[31] Duwadi, K.,2015, Design of ANN based MPPT for Solar Panel..
[32] Worku, M., and Abido, M., 2016, "Grid Connected PV System Using ANFIS Based MPPT Controller in Real Time," International Conference on Renewable Energies and Power Quality (ICREPQ 16), Madrid, Spain, May 4–6.
[33] Al-Majidi, S. D., Abbod, M. F., and Al-Raweshidy, H. S., 2019, "Design of an Efficient Maximum Power Point Tracker Based on ANFIS Using an Experimental Photovoltaic System Data," Electronics, **8**(8), p. 858.
[34] Hussein, H., Aloui, A., and AlShammari, B., 2018, "ANFIS-Based PI Controller for Maximum Power Point Tracking in PV Systems," Int. J. Adv. Appl. Sci., **5**(2), pp. 90–96.
[35] Abido, M., Khalid, M. S., and Worku, M. Y., 2015, "An Efficient ANFIS-Based PI Controller for Maximum Power Point Tracking of PV Systems," Arabian J. Sci. Eng., **40**(9), pp. 2641–2651.
[36] Al-Hmouz, A., Shen, J., Al-Hmouz, R., and Yan, J., 2011, "Modeling and Simulation of an Adaptive Neuro-Fuzzy Inference System (ANFIS) for Mobile Learning," IEEE Trans. Learn. Technol., **5**(3), pp. 226–237.
[37] Hakim, S. J. S., Razak, H. A., Allemang, R., De Clerck, J., Nieziecki, C., and Blough, J. R, 2012, *Topics in Modal Analysis I*, 5th ed., Vol. 5, Springer, New York, pp. 399–405.
[38] Bhatia, S., 2014, *Advanced Renewable Energy Systems (Part 1 and 2)*, CRC Press, New York.
[39] Bücher, K., 1997, "Site Dependence of the Energy Collection of PV Modules," Sol. Energy Mater. Sol. Cells, **47**(1–4), pp. 85–94.
[40] Kollimalla, S. K., and Mishra, M. K., 2014, "A Novel Adaptive P&O MPPT Algorithm Considering Sudden Changes in the Irradiance," IEEE Trans. Energy Convers., **29**(3), pp. 602–610.
[41] Nedumgatt, J. J., Jayakrishnan, K. B., Umashankar, S., Vijayakumar, D., and Kothari, D. P., 2011, "Perturb and Observe MPPT Algorithm for Solar PV Systems-Modeling and Simulation," 2011 Annual IEEE India Conference, Hyderabad, India, Dec. 16–18, pp. 1–6.